Antenna coupled photonic wire lasers

Tsung-Yu Kao,[1,*] Xiaowei Cai,[1] Alan W.M. Lee,[2] John L. Reno,[3] and Qing Hu[1]

[1]*Department of Electrical Engineering and Computer Science and Research Laboratory of Electronics, Massachusetts Institute of Technology, Cambridge, Massachusetts 02139, USA*
[2]*LongWave Photonics L.L.C., Mountain View, California 94043, USA*
[3]*Sandia National Laboratories, Center of Integrated Nanotechnologies, MS 1303, Albuquerque, New Mexico 87185-130, USA*
[*]*wilt_kao@mit.edu*

Abstract: Slope efficiency (SE) is an important performance metric for lasers. In conventional semiconductor lasers, SE can be optimized by careful designs of the facet (or the modulation for DFB lasers) dimension and surface. However, photonic wire lasers intrinsically suffer low SE due to their deep sub-wavelength emitting facets. Inspired by microwave engineering techniques, we show a novel method to extract power from wire lasers using monolithically integrated antennas. These integrated antennas significantly increase the effective radiation area, and consequently enhance the power extraction efficiency. When applied to wire lasers at THz frequency, we achieved the highest single-side slope efficiency (~450 mW/A) in pulsed mode for DFB lasers at 4 THz and a ~4x increase in output power at 3 THz compared with a similar structure without antennas. This work demonstrates the versatility of incorporating microwave engineering techniques into laser designs, enabling significant performance enhancements.

OCIS codes: (140.3300) Laser beam shaping; (250.5403) Plasmonics; (140.5965) Semiconductor lasers, quantum cascade; (140.3070) Infrared and far-infrared lasers.

References and links

1. J. P. Zhang, D. Y. Chu, S. L. Wu, S. T. Ho, W. G. Bi, C. W. Tu, and R. C. Tiberio, "Photonic-wire laser," Phys. Rev. Lett. **75**(14), 2678–2681 (1995).
2. M. I. Amanti, G. Scalari, F. Castellano, M. Beck, and J. Faist, "Low divergence Terahertz photonic-wire laser," Opt. Express **18**(6), 6390–6395 (2010).
3. M. A. Noginov, G. Zhu, A. M. Belgrave, R. Bakker, V. M. Shalaev, E. E. Narimanov, S. Stout, E. Herz, T. Suteewong, and U. Wiesner, "Demonstration of a spaser-based nanolaser," Nature **460**(7259), 1110–1112 (2009).
4. R. F. Oulton, V. J. Sorger, T. Zentgraf, R. M. Ma, C. Gladden, L. Dai, G. Bartal, and X. Zhang, "Plasmon lasers at deep subwavelength scale," Nature **461**(7264), 629–632 (2009).
5. H. Altug, D. Englund, and J. Vuckovic, "Ultrafast photonic crystal nanocavity laser," Nat. Phys. **2**(7), 484–488 (2006).
6. Q. Qin, B. S. Williams, S. Kumar, J. L. Reno, and Q. Hu, "Tuning a terahertz wire laser," Nat. Photonics **3**(12), 732–737 (2009).
7. E. E. Orlova, J. N. Hovenier, T. O. Klaassen, I. Kasalynas, A. J. Adam, J. R. Gao, T. M. Klapwijk, B. S. Williams, S. Kumar, Q. Hu, and J. L. Reno, "Antenna model for wire lasers," Phys. Rev. Lett. **96**(17), 173904 (2006).
8. M. T. Hill, Y.-S. Oei, B. Smalbrugge, Y. Zhu, T. de Vries, P. J. van Veldhoven, F. W. M. van Otten, T. J. Eijkemans, J. P. Turkiewicz, H. de Waardt, E. J. Geluk, S.-H. Kwon, Y.-H. Lee, R. Nötzel, and M. K. Smit, "Lasing in metallic-coated nanocavities," Nat. Photonics **1**(10), 589–594 (2007).
9. P. Bhartia, I. Bahl, R. Garg, and A. Ittipiboon, *Microstrip Antenna Design Handbook* (Artech House, 2001).
10. J. Faist, F. Capasso, D. L. Sivco, C. Sirtori, A. L. Hutchinson, and A. Y. Cho, "Quantum cascade laser," Science **264**(5158), 553–556 (1994).
11. R. Köhler, A. Tredicucci, F. Beltram, H. E. Beere, E. H. Linfield, A. G. Davies, D. A. Ritchie, R. C. Iotti, and F. Rossi, "Terahertz semiconductor-heterostructure laser," Nature **417**(6885), 156–159 (2002).
12. B. S. Williams, S. Kumar, H. Callebaut, Q. Hu, and J. L. Reno, "Terahertz quantum-cascade laser at $\lambda \approx 100$ μm using metal waveguide for mode confinement," Appl. Phys. Lett. **83**(11), 2124–2126 (2003).

#235869 Received 9 Mar 2015; revised 10 May 2015; accepted 12 Jun 2015; published 22 Jun 2015

13. M. I. Amanti, M. Fischer, G. Scalari, M. Beck, and J. Faist, "Low-divergence single-mode terahertz quantum cascade laser," Nat. Photonics **3**(10), 586–590 (2009).
14. T.-Y. Kao, Q. Hu, and J. L. Reno, "Phase-locked arrays of surface-emitting terahertz quantum-cascade lasers," Appl. Phys. Lett. **96**(10), 101106 (2010).
15. C. A. Balanis, *Antenna Theory: Analysis and Design.* (John Wiley & Sons, 2012).
16. S. Kumar, B. S. Williams, Q. Qin, A. W. Lee, Q. Hu, and J. L. Reno, "Surface-emitting distributed feedback terahertz quantum-cascade lasers in metal-metal waveguides," Opt. Express **15**(1), 113–128 (2007).
17. G. Xu, R. Colombelli, S. P. Khanna, A. Belarouci, X. Letartre, L. Li, E. H. Linfield, A. G. Davies, H. E. Beere, and D. A. Ritchie, "Efficient power extraction in surface-emitting semiconductor lasers using graded photonic heterostructures," Nat. Commun. **3**, 952 (2012).
18. G. Xu, L. H. Li, N. Isac, Y. Halioua, A. G. Davies, E. H. Linfield, and R. Colombelli, "Surface-emitting terahertz quantum cascade lasers with continuous-wave power in the tens of milliwatt range," Appl. Phys. Lett. **104**(9), 091112 (2014).
19. T.-Y. Kao, Q. Hu, and J. L. Reno, "Perfectly phase-matched third-order distributed feedback terahertz quantum-cascade lasers," Opt. Lett. **37**(11), 2070–2072 (2012).
20. D. Burghoff, T.-Y. Kao, D. Ban, A. W. M. Lee, Q. Hu, and J. Reno, "A terahertz pulse emitter monolithically integrated with a quantum cascade laser," Appl. Phys. Lett. **98**(6), 061112 (2011).
21. J. Faist, "Wallplug efficiency of quantum cascade lasers: critical parameters and fundamental limits," Appl. Phys. Lett. **90**(25), 253512 (2007).
22. A. Wei Min Lee, Q. Qin, S. Kumar, B. S. Williams, Q. Hu, and J. L. Reno, "High-power and high-temperature THz quantum-cascade lasers based on lens-coupled metal-metal waveguides," Opt. Lett. **32**(19), 2840–2842 (2007).
23. J. Lloyd-Hughes, G. Scalari, A. van Kolck, M. Fischer, M. Beck, and J. Faist, "Coupling terahertz radiation between sub-wavelength metal-metal waveguides and free space using monolithically integrated horn antennae," Opt. Express **17**(20), 18387–18393 (2009).
24. Y. Chassagneux, R. Colombelli, W. Maineult, S. Barbieri, H. E. Beere, D. A. Ritchie, S. P. Khanna, E. H. Lineld, and G. A. Davies, "Electrically pumped photonic-crystal terahertz lasers controlled by boundary conditions," Nature **457**, 174–178 (2009).
25. C. Bonzon, I. C. Benea Chelmus, K. Ohtani, M. Geiser, M. Beck, and J. Faist, "Integrated patch and slot array antenna for terahertz quantum cascade lasers at 4.7 THz," Appl. Phys. Lett. **104**(16), 161102 (2014).
26. F. Castellano, L. Li, E. H. Linfield, A. G. Davies, H. E. Beere, D. A. Ritchie, and M. S. Vitiello, "THz waveguide adapters for efficient radiation out-coupling from double metal THz QCLs," Opt. Express **23**(4), 5190–5200 (2015).
27. S. Heyminck, U. U. Graf, R. Güsten, J. Stutzki, H. W. Hübers, and P. Hartogh, "GREAT: the SOFIA high-frequency heterodyne instrument," Astron. Astrophys. **542**, L1 (2012).
28. Stratospheric Terahertz Observatory," (2012), http://soral.as.arizona.edu/STO/Welcome.html.

1. Introduction

Photonic wire lasers [1,2] and nano lasers [3,4] are new genres of laser structures that are of interests in applications such as ultrafast optical modulation [5] and frequency tuning [6]. However, the overall power extraction efficiency of these lasers are generally poor owing to their sub-wavelength cross sections [7]. One common feature of these laser structures is that metals are often used in order to achieve a high optical confinement even though the transverse dimension is in deep subwavelength, that is $w \ll \lambda$ [8]. To a certain degree, these waveguides can be viewed as microwave transmission lines operating at a much higher frequency. Following this analogy, we demonstrate a new type of laser structure with enhanced power extraction efficiency by coupling integrated antennas to the laser waveguide to form a distributed feedback structure.

The approach described in this letter is inspired by microwave engineering designs, where sub-wavelength slot antennas [9] are widely used in microstrip transmission line system. For those antennas, the microstrip waveguide consists of dielectric material sandwiched by a narrow metal strip and an infinite metal ground plane, and the antennas are formed by removing parts of the metal on the ground plane [see Fig. 1(a), left]. The missing ground plane causes a disruption of current flow along the transmission line in the ground plane, generating a net "in-plane" electric field across the gap, which produces far-field electromagnetic radiation. Thus, the rectangular opening becomes an effective antenna to extract power out from the microstrip transmission line. The shape and the position of this microstrip slot antenna can then be adjusted to maximize the power extraction efficiency, which is referred to as "impedance matching" in microwave engineering.

#235869 Received 9 Mar 2015; revised 10 May 2015; accepted 12 Jun 2015; published 22 Jun 2015

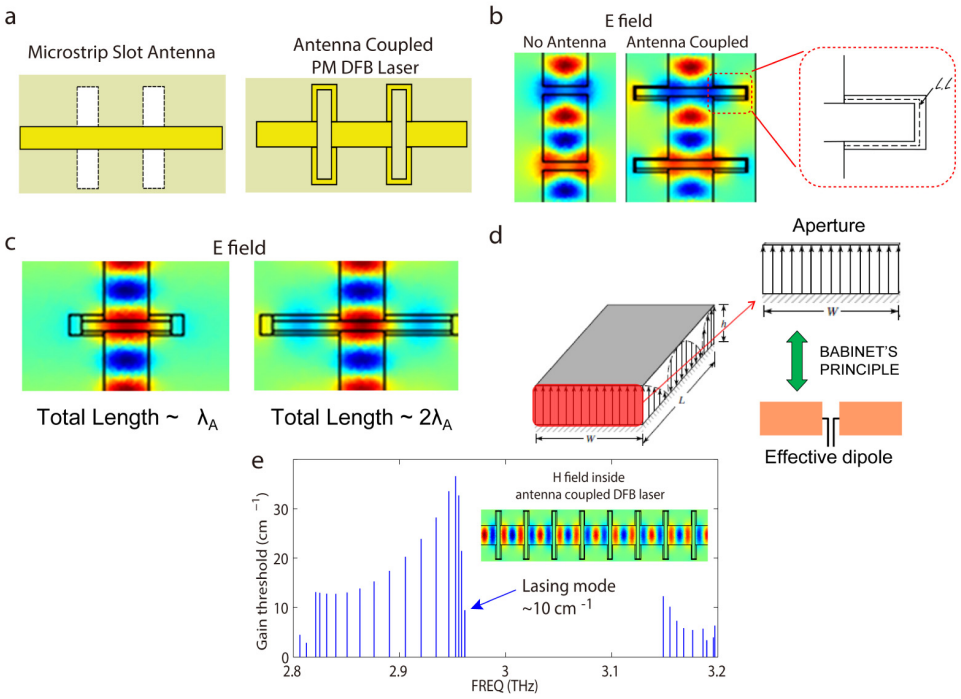

Fig. 1. (a) Schematic top views of slot antennas for microstrip transmission line (left) and antenna-coupled THz wire lasers (right). Top metal is in yellow while the bottom ground plane is in light green. (b) Electric field (E_z, where **z** is perpendicular to the metal planes) distributions for the same DFB laser with and without the coupled antenna structures. The area covered by the electric field with the same polarity is larger with the antenna-coupled structure. The definition of total antenna arm length *LL* is also illustrated. (c) Electric field distribution inside the cavity under different total antenna lengths. When the resonance condition is met, the field is virtually unchanged along the main laser cavity. (d) Schematics of one segment of DFB laser. The radiation comes from the facet "aperture antenna". The enhancement in radiation loss due to larger emission area can be understood through its effective dipole antenna model. (e) Lasing gain threshold versus frequency plot from finite element electromagnetic simulation of an antenna coupled DFB laser at 3 THz. The distance between adjacent antennas was chosen so that the third-order distributed feedback falls within the desired frequency. The magnetic field of the antenna-coupled laser is shown in the inset. The total antenna arm length *LL* ~λ_A.

2. Implantation in THz metal-metal waveguide QC lasers

2.1. Working principles and simulations

THz quantum cascade lasers (QCL) [10,11] in metal-metal waveguide [12], which is typically 10-μm thick and 20-30 μm wide, are chosen as the wire laser platform to incorporate the microstrip antenna. Instead of removing parts of the ground plane, which would require difficult fabrication process and also the extracted output power will be largely blocked by n^+ substrate, openings with rectangular shape are introduced on the top metal layer [Fig. 1(a), right] and the semiconductor beneath the opening are removed to expose the ground metal layer.

The integrated antenna creates additional paths for electromagnetic energy to transmit from one segment of cavity to another. The antennas can be regarded as two very narrow transmission lines folded into the shape of a horseshoe, connecting cavities on both sides of the gap. The dotted line in Fig. 1(b) depicts the total antenna arm length, *LL*, along the centerline of the antenna loop on one side of the DFB cavity. In order to assure that the additional transmission lines do not disrupt the desired operation of the distributed feedback

#235869 Received 9 Mar 2015; revised 10 May 2015; accepted 12 Jun 2015; published 22 Jun 2015

provided by the trench gap between adjacent cavities, the physical dimensions of the antenna structure need to be carefully designed. Using 3-D full-wave finite element method (FEM) simulation, quasi-eigenmodes of the whole antenna-coupled wire laser structure can be found with detailed information of both electric and magnetic field distributions. Knowing the eigenfrequencies and the corresponding radiation losses, we can then estimate the lasing frequency and calculate far-field beam patterns. The simulations were carried out using COMSOL Multiphysics version 4.3. No metal losses and material losses were taken into account when performing the "cold cavity" eigenmode simulation. The simulation environment was surrounded with perfect-matching layer (PML) to absorb unphysical reflections from the boundaries.

Figure 1(c) shows the electric field inside a laser cavity operating at the third-order feedback [13]. Note that the polarity of the electric field is the same on both sides of the gap. In order to satisfy this boundary condition, the total length of the antenna arm *LL* has to meet the following requirement:

$$LL = \lambda_A \times m \tag{1}$$

where m is an integer number = 1, 2, 3, ..., and λ_A is defined as the wavelength of the mode traveling along the narrow antenna arm. This requirement is similar to the resonance condition for phase-locking two DFB lasers as described in [14]. The resonance condition can be verified by attaching antennas with two different resonant lengths ($LL = 1 \times \lambda_A$ and $2 \times \lambda_A$). As shown in Fig. 1(e), it is clear that the electric field distributions inside the DFB cavity are virtually identical and the third-order grating condition is evidently undisturbed when the total antenna length equals to integer multiples of λ_A.

The increase in radiation efficiency can be attributed to the effectively larger emitting facet cross section. Figure 1(d) (shaded in red) shows the electric field distribution on one of the many facets of a DFB laser structure. Based on the "Babinet's Principle" [15], one can replace this aperture antenna with its equivalent dipole antenna. Thus, a laser ridge with $w \ll \lambda$ will be analogous to a short dipole antenna with the radiation resistance $R_{rad} \propto (w/\lambda)^2$. $w \ll \lambda$ is the characteristic of photonic wire lasers, and also a condition often met in THz lasers based on metal-metal waveguides, leading to their poor power extraction efficiency. As shown in Fig. 1(c), after attaching the antenna, the electric field at the gap extends into the antenna arm, which enlarges the length of the effective dipole antenna (w), leading to more efficient emission. We would like to point out that although the antenna structures bear resemblance to the traditional microstrip antennas, their working principals are not entirely the same. For antenna-coupled third-order DFB lasers, the radiation originates from the strong electric field Ez (which is perpendicular to the metal planes) along facets, while for microstrip antennas, radiations are mainly generated by the electric field across the metal opening (along longitudinal direction). The latter case resembles antenna-coupled DFB lasers of even orders and will be discussed in the Section 3.2.

Figure 1(e) shows the full-wave finite element method electromagnetic simulation for an antenna-coupled wire laser designed at 3 THz with a total antenna arm length *LL* ~λ_A. When compared with the devices without the extra loop antenna, the loss value of the eigenmode with the lowest radiation loss (thus the lasing mode) increases from 3 cm^{-1} to ~10 cm^{-1} which will yield a ~3 × increase of power extraction efficiency. Similar enhancement in radiation losses can also be found in simulations for antenna-coupled devices at other frequencies.

2.2. Experimental results

Figure 2(a)-2(c) show the continuous-wave/pulsed *I-V* and *L-I* curves and spectra data of the antenna-coupled wire lasers centering at ~2, ~3, ~4 THz respectively with different antenna arm lengths.

#235869 Received 9 Mar 2015; revised 10 May 2015; accepted 12 Jun 2015; published 22 Jun 2015

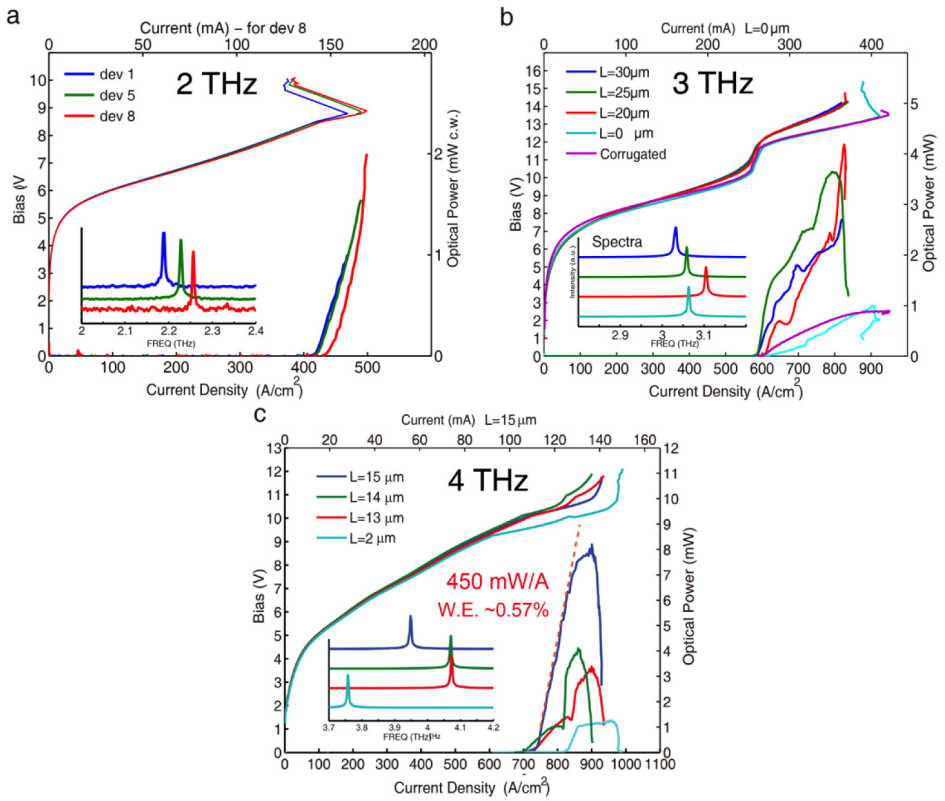

Fig. 2. *I-V* curves, *L-I* curves and spectra data of antenna-coupled THz wire lasers at different frequency bands (*cw* or pulsed). (a) Results of antenna-coupled lasers designed around 2 THz (*cw*). Device 1, 5 and 8 have the same total antenna arm length but with different cavity periodicities which results in a linear frequency scaling. (b) Results of antenna-coupled lasers designed around 3 THz (pulsed). All lasers have the same cavity periodicity but different antenna arm lengths—L = 0, 20, 25, 30 μm. L = 0 μm is a special case where the distance between the end of antenna loop and the edge of the main laser ridge is eliminated and thus the antenna arm length equals to zero. The fact that DFB lasing frequency changes with the length of antenna arm indicates a strong coupling between antennas and the waveguides. Results from a conventional corrugated third-order DFB laser is also shown as a comparison. (c) Results of antenna-coupled lasers designed around 4 THz (pulsed) with measurement data of 25-period antenna-coupled lasers (~3.95 THz). The upper axis is plotted against the current of the device with antenna arm length L = 15 μm. This device shows ~450 mW/A pulsed slope efficiency and 0.57% wall-plug efficiency. Measurements for devices with different antenna arm lengths are also shown. We contributed the lower power from devices with L = 13 and 14 μm to their higher lasing frequency (4.1 THz), which is away from the peak gain frequency (~3.9 THz) of the gain medium. The disrupted changes in L-I curves for these devices also indicate mode-hopping behaviors. All spectra shown in Fig. 2 were measured near the peak power bias condition, where single-mode emissions are observed.

Figure 2(a) shows *cw* L-I-V curves for antenna-coupled wire lasers at 2 THz. At this long wavelength, the radiation resistance is significantly reduced, so it is essential to implement the integrated antenna structures in order to efficiently extract power. From FEM simulation, the radiation loss increases by a factor of ~5, from 1.4 cm^{-1} to 6.7 cm^{-1}, after the introduction of the antenna. All lasers have the same 23-μm antenna arm length, but with slightly different cavity lengths. Device #8, an 18-μm wide, 30-period device (~2-mm long) emits 1.9 mW continuous-wave power at 2.25 THz at 14 K with maximum lasing temperature T_{max} = 80.6 K (pulsed). The slope efficiency of this laser is around 100 mW/A with 0.12% wall-plug

#235869 Received 9 Mar 2015; revised 10 May 2015; accepted 12 Jun 2015; published 22 Jun 2015

efficiency, which is believed to be the highest efficiency DFB laser at this low frequency range.

Figure 2(b) shows the pulsed I-V and L-I curves and spectra data of antenna-coupled 3-THz lasers with different antenna arm length L along with traditional corrugated DFB laser from the same gain medium and fabrication. The maximum lasing temperatures T_{max} are 134 K (pulsed) and 105 K (*cw*) for laser with antenna arm length L = 20 μm. This 31-μm wide, 31-period (1.5-mm long) device emits ~4 mW of pulsed power at 10 K. In comparison, the data from a corrugated DFB laser [2] with similar dimensions and fabricated from the same gain medium is also shown. Power increases by roughly 4 times when compared with the conventional corrugated DFB laser after normalization against their biasing currents. However, the slope efficiency of the antenna-coupled device at 3 THz is merely ~45 mW/A, with 0.08% WPE. After comparing this result with previous power measurements of two metal-metal waveguide Fabry-Pérot lasers (with Winston cone to improve collection efficiency) fabricated using the same gain medium wafer: 10 mW from a 170 μm x 1.24 mm device (1.98A, 15V, wall-plug efficiency (WPE) = 0.033%) and 6 mW from a 100 μm x1.7 mm device (1.53A, 15V, WPE = 0.026%), it is concluded that the gain medium used for the 3 THz laser inherently gives lower power output. Despite a relatively low efficiency, the antenna-coupled laser still shows 2 to 3 times improvement in WPE over Fabry-Pérot lasers, which a solid proof that the out-coupling efficiency has been greatly enhanced using the coupled antenna approach.

Figure 2(c) shows the pulsed *I-V* and *L-I* curves and spectra data of antenna-coupled 4-THz lasers with different antenna arm lengths. For a 22-μm wide, 25-period device (~1-mm long) with 15-μm antenna arm length, it reaches >8 mW pulsed power (10% duty-cycle) at 12 K with maximum lasing temperature T_{max} = 109 K (pulsed) and > 77 K (*cw*). Limited by the instrument used at the time of the experiment being conducted, the *cw* power was not measured. However, no noticeable reduction in pulsed power was observed when varying the pulse width from 1 μs to 1 ms with fixed 10% duty-cycle, indicating good thermal removal due to the narrow width of the device (22-μm). The lasing frequency is ~3.95 THz throughout the entire bias range. The lasing threshold for the laser is ~730 A/cm^2 with maximum power delivered at ~900 A/cm^2 (130 mA, 10.8 V) yielding a 0.57% pulsed wall-plug efficiency. The slope efficiency of the same device is ~450 mW/A near the lasing threshold (dotted red line in the figure), which is the highest slope efficiency for THz DFB lasers with single-mode operations [2,16–18]. It is worth pointing out that since the antenna coupled laser emits the same amount of THz radiation at both front and back directions, a factor-of-two improvement in power could be readily achieved by collecting THz power from both sides of the device.

In designing antenna-coupled lasers, due to the now largely enhanced radiation loss (α_m) (from 3 to 5 cm^{-1} to 10-18 cm^{-1}) for the designed mode, the gain medium might not have enough gain to support the designed high radiation loss mode under low bias voltage. Other lower loss modes will become the lasing mode first until the peak frequency starts to align with the designed high radiation loss mode. Although one laser might go through several mode-hops (see the discontinuities in the light-current curves for antenna-coupled lasers at 3 and 4 THz) before reaching its maximum power, single mode emission is still achieved near peak power.

#235869 Received 9 Mar 2015; revised 10 May 2015; accepted 12 Jun 2015; published 22 Jun 2015

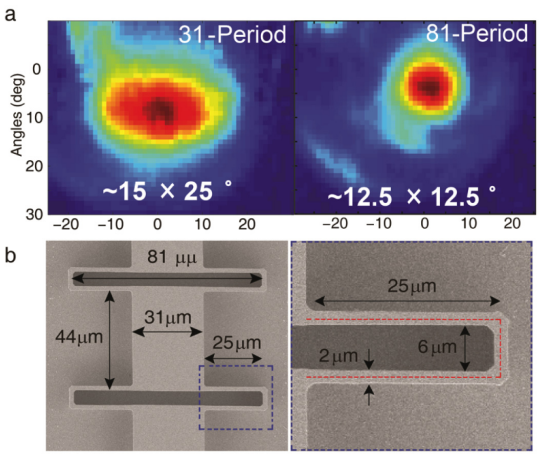

Fig. 3. (a) Measured beam patterns from two antenna-coupled lasers around 3 THz with the same antenna arm length L = 25 μm, but different total device lengths (31-period and 81-period, corresponding to 1.5 mm and 4 mm). (b) Scanning electron microscopy (SEM) pictures (top view) for a 3 THz antenna-coupled wire laser with antenna arm length L = 25 μm. The right side of one of the antenna loops is shown in the zoom-in picture. The dashed red line depicts the total antenna arm length *LL*. *LL* ≈56 μm ≈$\lambda_A = \lambda_0/n_A$ ≈(100 μm)/n_A, where n_A is the effective waveguide index of the 2-μm antenna ridge. The dimensions of each segment of laser cavity are 31 × 44 μm with a 6-μm gap size.

Figure 3(a) shows the measured far-field beam patterns of a 31-period (1.5-mm long) device and an 81-period (4-mm long) device that lases at ~3 THz. The former device has a beam divergence 15 × 25° and the latter with a narrower and a more symmetric beam divergence 12.5 × 12.5°. The corresponding output power of the laser scales linearly with the device length. The symmetric and low divergence beam pattern is attributed to the third-order grating condition as described in [13] and the power scalability originates from a nearly perfect phase-matching condition [19]. Both conditions could be met using the antenna-coupled laser structure. Figure 3(b) shows the SEM picture of one of the antenna-coupled wire laser along with detailed dimensions.

For pulsed *L-I-V* measurement, the lasers are operated at 20 kHz with 400 ns pulse duration (0.8% duty cycle) at temperature 10 K. The THz light output is measured with liquid helium cooled Ge:Ga photodetector. For continuous-wave measurement, the optical power is measured with a pyroelectric detector with mechanical chopping at 100 Hz. Spectra are measured using a Fourier transform infrared spectrometer (FTIR, model: Thermo Nicolet 6700) with liquid helium cooled Ge:Ga photodetector as external detector. The laser is operated near its peak power.

THz optical power is measured without any focusing optics between the laser and the power meter except a HDPE window on the cryostat. Pulsed measurement is performed using Thomas-Keating absolute Terahertz power meter at a 30-Hz electronic chopping frequency. The laser under test is operated at 100 kHz with 1 μs pulse duration (10% duty-cycle) at temperature 10-12 K inside Cryomech Pulse tube cryorefrigerator model PT 810. For continuous-wave power measurement, thermopile power meter (ScienTech model AC2500H) is used. All power measurement is done in atmosphere without purging. Far-field beam patterns are measured with a pyroelectric detector mounted on a two-dimensional motorized scanning stage which is placed at 20 cm from the device. Laser is operated near the peak power in pulsed mode at 100 kHz with 1 μs pulse duration and then gated with another 100 Hz signal.

#235869 Received 9 Mar 2015; revised 10 May 2015; accepted 12 Jun 2015; published 22 Jun 2015

2.3 Fabrication method

Due to uncertainties in fabrication, a series of antenna-coupled wire lasers with the same cavity and gap dimensions but different antenna lengths are fabricated on a single chip. The biasing current is first provided to the laser through a bonding pad connected to the last section of the DFB laser and then through antenna loops to the entire laser structure. After preforming the standard Au-Au wafer-bonding process used in THz QC lasers and removing the residue substrate to expose the active medium by wet etching in citric acid, a thin SiO_2 layer is blankly deposited on the wafer and then patterned to provide electrical isolation for the bonding pad. Standard contact lithography with image reversal photoresist AZ 5214 is then used to form Ti/Au metal mask on top of the active region. Area that is not masked by the Ti/Au pattern is then etched using inductive coupled plasma reactive ion etcher (ICP-RIE) in $SiCl_4$ chemistry until the bottom metal plane is exposed. In Fig. 3(b) and Fig. 4(b), good lithographic resolution and dry etch quality are clearly visible.

The active material is based on molecular beam epitaxy (MBE) grown $GaAs/Ga_{0.85}Al_{0.15}As$ multiple quantum well structure. The thickness of the gain medium is 10 μm. Design FL175M-M3 (a 4-well resonant-phonon design), wafer number EA1222 is used for 2 THz devices. Design OWI-180E (a 3-well resonant-phonon design), wafer number VB0205 is used for 3 THz devices and Design FL183S (a 4-well resonant-phonon design), wafer number VB0481 is used for devices around 4 THz.

3. Other discussions

3.1 The effect of antenna shape

Antennas in different geometric shapes are also investigated using the finite element electromagnetic simulation. Figure 4(a) shows two different antenna types for laser cavity at 4 THz. In Type I configuration, two longer arms of antenna are brought in closer and in Type II configuration, those arms are separated with larger distance. FEM simulations show Type I configuration yields ~30 cm^{-1} in radiation loss while Type II yields ~18 cm^{-1}. Since the measured lasing threshold of a Fabry-Pérot laser is ~18 cm^{-1}, which is largely due to material loss in the waveguide [20], Type II structure is chosen for the 4 THz laser cavity in order to maximize wall-plug efficiency. SEM picture of a fabricated Type II antenna structure is shown in (b).

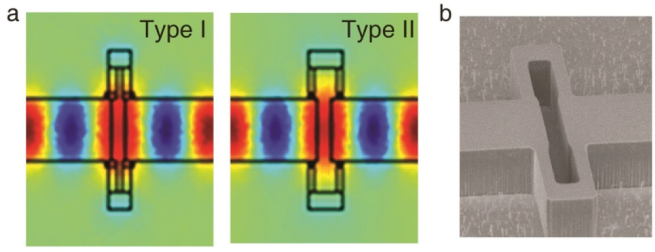

Fig. 4. (a) Electric fields from FEM simulations of two different configurations of antenna structure. In Type I, two longer arms of antenna are brought in closer while in Type II, those arms are separated with larger distance. (b) SEM picture of Type II antenna.

3.2 Other operation modes

It is worth pointing out similar enhancement in out-coupling efficiency can also be observed in second-order or higher even-order surface-emitting DFB lasers, by choosing a different resonance condition:

$$LL = \left(m - \frac{1}{2} \right) \lambda_A, \tag{2}$$

#235869 Received 9 Mar 2015; revised 10 May 2015; accepted 12 Jun 2015; published 22 Jun 2015

where *LL* is the total antenna length defined in the main article and m = 1, 2, 3, ... When this condition is met, the z-component of electric fields on each side of the cavity gap will have opposite polarities, as illustrated in Fig. 5(a). Under this circumstance the field distribution near the antenna will resemble the traditional slot antennas used in microstrip transmission line. The technique of coupled antennas can be also adopted by other surface-emitting laser such as the graded photonic heterostructures laser [17,18] when operated under this alternate resonance condition.

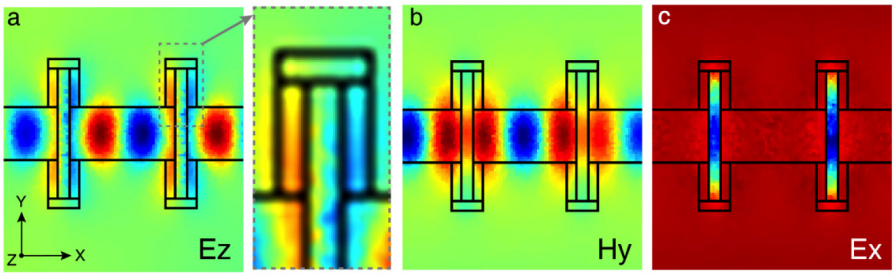

Fig. 5. (a) Electric and (b) magnetic fields from FEM simulations when Eq. (2) is met. The zoom-in picture of the electric field distribution in (a) shows the opposite polarity on both ends of the antenna arms and $LL \approx 0.5\,\lambda_A$. (c) Strong electric fields parallel to the metal surfaces (Ex) can be found across the antenna when the structure is operated under this condition. This strong Ex, together with a strong Hy over a large "slot" area, will result in a strong radiation toward the normal (z) direction.

3.3 Discussions on wall-plug efficiency and slope efficiency

The wall-plug efficiency (WPE) of a laser is defined as the ratio between the output optical power and the total electrical power consumed by the device. For any quantum cascade laser, under simple rate equation analysis, its wall-plug efficiency (WPE) can be expressed in the following equation [21]:

$$WPE \approx \frac{optical\ power}{V \cdot I} = \eta_i \cdot N \cdot \frac{\hbar\omega}{q} \cdot \frac{\alpha_m}{\alpha_w + \alpha_m} \cdot \frac{I_{max} - I_{th}}{V_{max} \cdot I}, \qquad (3)$$

where V_{max} is the bias voltage when the maximum power is delivered from the laser, I_{max} is the maximum bias current, and η_i is the current injection efficiency of the quantum well structure which takes into account the dark current that does not go through the optical transition. N is the number of modules in the QCL, $\hbar\omega$ is the energy per photon, and q and the electron charge. α_m is the mirror loss of the laser cavity, which is defined as the total radiation loss per round-trip when light is traveling inside the cavity. α_w is the waveguide loss and $\alpha_w + \alpha_m$ would be the total loss of the laser. For the sake of simplicity, the effect of confinement factor is not included in the equation. I_{th} is the lasing current threshold of the device. This equation basically assumes, for every second, $\eta_i \cdot (I_{max} - I_{th})/q$ of electrons go through N cascade optical transitions of the multiple quantum wells structure and each one of the transition emits a photon with $\hbar\omega$ energy. A photon has a probability of α_m over $(\alpha_w + \alpha_m)$ to survive the loss in the waveguide and then escape from the cavity to be detected by the power meter.

We can rearrange the previous equation into

#235869 Received 9 Mar 2015; revised 10 May 2015; accepted 12 Jun 2015; published 22 Jun 2015

$$WPE = \left(\eta_i \cdot N \cdot \frac{\hbar\omega}{q} \cdot \frac{\alpha_m}{\alpha_w + \alpha_m} \right) \cdot \frac{I_{max} - I_{th}}{I} \cdot \frac{1}{V_{max}} = Slope\ Efficiency \times Dynamic\ Range \times \frac{1}{V_{max}},$$

where

$$Slope\ Efficiency\ (SE) \equiv \left(\eta_i \cdot N \cdot \frac{\hbar\omega}{q} \cdot \frac{\alpha_m}{\alpha_w + \alpha_m} \right) \quad (4)$$

There are mainly two types of gain medium designs currently used by THz QCL community: Resonant-Phonon (RP) and bound-to-continuum (BTC). While having similar current injection efficiency and number of modules (η_i and N), BTC design has much lower maximum bias voltage V_{max} and current density (<5-6V, <500 A/cm^2, compared with 12-15V, ~1000 A/cm^2 in RP design) and thus dissipates less electrical power which will lead to higher WPE under same SE.

A direct comparison of wall-plug efficiency between different devices will be skewed by the type of gain medium design used among different research groups due to the huge disparity in maximum bias voltage. Hence, the parameter WPE is not an indicative parameter of power extraction efficiency of emitting structures. If we focus on the slope efficiency, which measures the ability to extract power out from the laser cavity, a significant improvement has been made using the antenna-coupled cavity. We reported SE ~450 mW/A at 3.95 THz which increased ~2 times when compared with ~200-250 mW/A at 3.4 THz for photonic heterostructure device [17,18], and 150-230 mW/A at ~3 THz for the original THz photonic wire laser [2,13].

4. Conclusions

In conclusion, we have demonstrated a new type of laser, which is a hybrid of microwave engineering technology with distributed gain media. This structure utilizes antennas as both feedback enhancers and radiation emitters. At THz frequency range, this antenna-coupled laser generates highly efficient single-mode *cw* THz radiations with symmetric and low-divergence beam patterns. With this hybrid antenna-coupled lasers, we have achieved the highest pulsed slope efficiency (450 mW/A) in single-mode THz DFB lasers when compared with other laser cavity designs used in THz lasers [16–20,22–26]. A pulsed wall-plug efficiency of 0.57% is also achieved. Furthermore, the new structure does not require any additional fabrication steps beyond those for DFB or Fabry-Pérot lasers, in contrast to horn-, fiber-, waveguide-, or lens-coupled lasers [20,23,26]. The narrow width in both the antennas and ridges allows efficient heat removal, which is essential for *cw* operations. This highly efficient antenna-coupled THz laser would be ideal for applications such as local oscillator for heterodyne receiver in SOFIA/GREAT [27] and STO [28]. Similar technique can also be applied to other frequencies by scaling the dimensions and also by using dielectric antennas.

Acknowledgments

This work is supported by NASA and NSF, and also performed at the Center for Integrated Nanotechnologies, a U.S. Department of Energy, Office of Basic Energy Sciences user facility. Sandia National Laboratories is a multi-program laboratory operated by Sandia Corporation, a wholly owned subsidiary of Lockheed Martin Corporation, for the U.S. Department of Energy's National Nuclear Security Administration under contract DE-AC04-94AL85000. T-Y.K. conceived the strategy, designed and fabricated the devices, and performed the measurements and analysis. X.C. designed, fabricated, and performed the measurements of the 2 THz devices. A.L. contributed to the original idea of antenna-coupled wire laser. J.L.R. provided the material growth. All the work was done under the supervision of Q.H.

#235869 Received 9 Mar 2015; revised 10 May 2015; accepted 12 Jun 2015; published 22 Jun 2015